Suspended sediment properties in the Lower Mekong River, from fluvial to estuarine environments

Hoang-Anh Le, Nicolas Gratiot, William Santini, Olivier Ribolzi, Duc Tran, Xavier Meriaux, Eric Deleersnijder, Sandra Soares-Frazão

Suspended sediment properties in the Lower Mekong River, from fluvial to estuarine environments

Hoang-Anh Le [1,2], Nicolas Gratiot [2,3,*], William Santini [4], Olivier Ribolzi [4], Duc Tran [5], Xavier Meriaux [6], and Eric Deleersnijder [7,8], Sandra Soares-Frazão [1]

[1] Civil and Environmental Engineering, Institute of Mechanics, Materials and Civil Engineering (IMMC), Université catholique de Louvain, Place du Levant 1, B-1348 Louvain – la – Neuve, Belgium
[2] Asian Research Center on Water (CARE-Rescif), Ho Chi Minh City University of Technology, Block B7, 268 Ly Thuong Kiet Street, District 10, Ho Chi Minh City, Vietnam
[3] CNRS, IRD, IGE, Université Grenoble Alpes, F-38000 Grenoble, France
[4] Géosciences Environnement Toulouse (GET), Université de Toulouse, IRD, CNRS, UPS, Toulouse, France
[5] Faculty of Environment and Natural Resources, Ho Chi Minh City University of Technology, VNU-HCM, 268 Ly Thuong Kiet, Ho Chi Minh City, Vietnam
[6] Université Littoral Côte d'Opale, Université Lille, CNRS, UMR 8187, LOG, Laboratoire d'Océanologie et de Géosciences, F 62930Wimereux, France
[7] Université catholique de Louvain, Institute of Mechanics, Materials and Civil Engineering (IMMC) & Earth and Life Institute (ELI), 4 avenue Georges Lemaître, B-1348 Louvain-la-Neuve, Belgium
[8] Delft University of Technology, Delft Institute of Applied Mathematics (DIAM), Van Mourik Broekmanweg 6, 2628XE Delft, The Netherlands

* Correspondence: nicolas.gratiot@ird.fr; Tel.: +84-9-4129-4232

Abstract: The Mekong river is one of the largest rivers in the world, which flows through six countries of Southeast Asia (China, Myanmar, Laos, Thailand, Cambodia and Vietnam). Its hydro-sedimentary regime is changing rapidly, as a consequence of a regional shift of land use (agriculture, road, etc.), damming, sand mining and climate changes, among others. This study assesses the behavior of particles transported in suspension in the Lower Mekong River (LMR), along approximately 1700 km from fluvial to estuarine environments. Suspended sediment properties were estimated, simultaneously with hydrodynamic conditions, during three field campaigns. In addition, further investigations were performed in the laboratory to assess the structures of particles (flocculated or not), their capacity to flocculate (and the impacts on siltation), under a wide range of sediment concentration (400 to 4000 $mg.L^{-1}$). This study confirms that suspended sediment transported in the LMR are predominantly (75 % by volume) flocculi (or freshly eroded soils aggregates), with median

aggregated particle size in the range 10 - 20 µm and median settling velocity of the order of 0.01 – 0.1 mm.s^{-1}. These flocculi are robust under the hydrodynamic conditions (turbulence and suspended sediment concentration – SSC) existing in the LMR. Laboratory investigations reveal the existence of a threshold sediment concentration (400 mg.L^{-1}), beyond which flocculation and sedimentation increase of orders of magnitudes. Thus, concentration that exceeds this threshold might promote the formation of so-called fluid mud layers. Because of the nonlinear response of flocculation and sedimentation with SSC and considering the ongoing changes at a regional scale in the LMR, higher occurrence of fluid mud layers in the fluvial upstream waterbodies might be anticipated, and a lower occurrence in estuaries and alongshore where the concentration decrease. The geomorphology could be impacted, with an over-siltation in dams and an exacerbated erosion of the muddy-mangrove coast.

Keywords: Mekong; LISST; SCAF; fluid mud layer; flocculation, settling velocity

1. Introduction

The Mekong river is the tenth longest river in the world with a length of 4909 km and has a basin area of 795,000 km^2. Its mean annual discharge is approximately 475 km^3, i.e. the sixth largest in the world. The river originates from the Tibetan Plateau (China) with an elevation of more than 5000 m above sea level (a.s.l.); then, the river flows through a variety of geomorphological and climatic systems and ends in the fertile delta of Vietnam (55,000 km^2), before discharging into the South East Sea of Vietnam (Mekong River Commission portal - MRC, www.mrcmekong.org/). Under human pressures and climate change, the river is facing many serious issues in link with changes in sediment dynamics. One of the most evident transformation is the construction of large hydropower dams in the upstream Mekong, which are modifying the hydrological cycle, and reducing the sediment discharge into the floodplain and estuaries at an alarming point (Schmitt et al., 2017). Sand mining in the delta is also a direct threat for the hydro-sedimentary budget. According to the literature, sediment flux has already decreased by almost five fold over 35 years, from about 160 mill. tons.year^{-1} in 1983 (Milliman et al., 1983) to 87.4 ± 28.7 mill. tons.year^{-1} in 2005 (Darby et al., 2016 and Schmitt et al., 2017) and 40 ± 20 mill. tons.year^{-1} in 2015 - 2016 (Thi Ha et al., 2018).

Sand mining, trapping by dams, and the resulting reduction of sediment flux are undoubtedly corroborated with some changes in the nature (and populations) of particles transported. Some expected consequences in geomorphology, floodplain fertility and pollutant dynamics are already evoked (Kondolf et al., 2018), but need to be better studied. Previous studies conducted in the LMR indicated that the upper fluvial section was dominated by two particles size populations: silts, with a diameter of 10 - 20 µm; and sands, with a diameter of 63 - 200 µm, accounting for 78 % and 22 % of the total particle load, respectively (Peteuil et al., 2014). Downstream, in the estuary, flocculated fine particles dominate. The observed floc size, reported in the literature, was 30 - 40 µm, constituting 60 - 80 % of the total sediment load in high flow season. However, in the low flow season, the floc size increased to 50 - 200 µm, accounting for 70 - 80 % of the total volume (Wolanski et al., 1996 and Wolanski et al., 1998). This observed variability of sediment properties reflects a direct adjustment of physical properties along streams, which operates at microscopic scales (flocculation, sedimentation and erosion), in link with hydrodynamic conditions and their seasonal variations. The different origins, together with different physicochemical and biological conditions between the sites, cause difficulties in interpreting the results.

Particle size, settling velocity and their spatio-temporal evolution through flocculation, are fundamental properties that need to be estimated to assess sediment transport and deposition processes in space and time (Manning et al., 2011a; Winterwerp, 2002). This is particularly true in the case of mud/sand mixtures, where complex interactions occur and need to be characterized for a realistic understanding of sediment dynamics (Manning et al., 2010). Conceptually, flocculation develops from primary particles into hierarchical structures, namely flocculi, microflocs and macroflocs. Primary particles mainly consist of fine particles with sizes of 1 - 6 µm, and can be organic or inorganic. They aggregate to form 1st order structures, so-called flocculi, with diameters of the order of 6 - 50 µm. They are usually hardly broken down into primary particles, even at the highest turbulent shear modulus experienced by particles in large rivers. Thus, it is generally considered that flocculi are a major component of sediment dynamics. Microflocs form the 2nd order of aggregation. They include primary particles and flocculi and have sizes of 50 - 200 µm. Finally, macroflocs are the largest particle structures. They are loose structures with a wide size distribution, ranging from hundreds to thousands of micrometers (Lee et al., 2012 and Fettweis et al., 2006). Flocs (micro and macro) are generally fragile structures, easily broken down when passing through high turbulent shear modulus (Manning et al., 2011a).

Flocculation at microscopic scale, as some hydro-sedimentary and geomorphological impacts at scales of river reaches, estuaries and deltas, in particular because it promotes the formation of fluid mud layers. Fluid mud is defined as a mixture of high-concentrated fine sediments with water (Bachmann et al., 2005). It is generated by liquefaction of cohesive sediment beds by waves or by an imbalance between settling and eddy diffusion near the bed, or by the convergence of sediment fluxes from upstream and downstream. In energetic environments, large particles such as sand are also found in fluid mud samples, but the portion is less than few percent (McAnally et al., 2007). Fluid mud masses may be advected over large distances horizontally without losing their coherent nature or internal chemical properties; and its horizontal convergence may often be a key mechanism of their accumulation (McAnally et al., 2007). Thus, fluid mud in thin layers is considered as an intermediate stage of deposition (before formation of consolidated bed layers) or bed erosion (under entrainment process by fluidization (McAnally et al., 2007). Its thickness varies from few centimeters to meters (Sottolichio et al., 2011; Azhikodan et al., 2018).

The occurrence of fluid mud is commonly observed in quiescent environments such as lakes and reservoirs (Mehta et al., 1991; McAnally et al., 2007) or in the Estuarine Turbidity Maximum zones (ETM) (Uncle et al., 2006; Winterwerp et al., 2011; Azhikodan et al., 2018) such as estuaries, navigation channels, harbour basins or along muddy coasts all over the world (Bachmann et al., 2005; Schelske et al., 2006; Gratiot et al. 2007; Toorman et al. 2018). The turbidity maximum zone is often created by resuspension from the bed during parts of the tidal cycle and shows a significant drag reduction at high SSC concentration gradient (Dyer et al., 2002a and Dyer et al., 2002b). However it has been poorly studied and reported in the literature dedicated to the LMR (Wolanski et al., 1998, Xue et al., 2010) and received some more interest recently (Gugliotta et al., 2019; Nittrouer et al., 2017; Gratiot et al., 2017).

This study originally combines in situ measurements and laboratory investigations to examine the physics of particles (especially flocculation properties, measured with new patented equipment developed by SCAF®) and to understand transport/deposition processes in the LMR. Sampling and analyses are performed in three contrasted environments: an upper fluvial reach in Laos (Fig. 1b), a lacustrine environment in Cambodia (Fig. 1c) and an estuarine environment in Vietnam (Fig. 1d). The same methodology was applied for these three contrasted environments (upstream river, lake and estuary). Results obtained allow for answering and discussing the following points:

- Are suspended sediment flocculated or not (percentages of cohesive versus non-cohesive particles transported in suspension)?

- If yes, are floc populations stable from upstream to downstream and/or highly dependent on hydrodynamic conditions (SSC, turbulence, salinity)?

- Are suspended sediment predominantly transported as washload (single path with no bed interactions), or does it experience successive phases of deposition and erosion?

- How much SSC increase can modify flocculation, sedimentation and how much this could contribute to the formation of fluid mud layers and, finally, modify the geomorphology of the LMR?

By answering to the four questions above, the paper proposes a better understanding of the physical properties of sediment and their transportation modes along the Lower Mekong River. Because flocculation and fluid mud layers are playing an important role in the dynamic of the Mekong Delta, this information will facilitate the implementation of integrated tools, such as ecological/geomorphological models, to go through a better management of large scale hydrosystems.

2. Study areas and Methods

2.1. Study area

Field investigations have been conducted at three locations of the LMR, assumed to be representative of river morphological units, from the upper fluvial environment to the lacustrine and the estuarine environments (Fig. 1a).

2.1.1. Fluvial environment

The upper fluvial reach considered is located at the level of Luang Prabang city, Laos (Fig.1b). It is situated on a long stem at the confluence of the Mekong and Nam Khan rivers, a tributary of the Mekong. Its altitude is approximately 300 m a.s.l. This area is covered with steep hillsides and has been experiencing drastic land use changes, predominantly leading to erosion, since the last decades (Ribolzi et al., 2017). At Luang Prabang, the Mekong river section is already wide, with width of 600 - 700 m. However, when passing through gorges, the channel becomes swiftly narrow, approximately 100 m wide, and bounded by limestone

159 pavement. The channel has a median depth of around 10 m, with maximum depth of
160 approximately 30 m (Gupta et al., 2007).
161 The field survey was conducted for 8 days, from 26 June to 2 July 2017, at the beginning of
162 the wet season. There were neither extreme floods nor low water situations, thus the
163 hydrodynamic conditions were suitable for sampling and analysing a typical (median)
164 suspended sediment distribution in the river. Twenty-seven samples were taken in the main
165 Mekong river and its tributaries (Nam Ou, Nam Suang and Nam Khan tributaries). During the
166 survey, hydro-sedimentary conditions were also characterized on two cross-sections with
167 distances of approximately 20 km (Fig. 1a, see section 2.2.3). For each location, samples were
168 collected in three vertical profiles (left bank – V1, middle bank – V2 and right bank – V3). In
169 each vertical profile, 3 litres of water sample were taken at various depths (0.1 h, 0.4 h, 0.7 h
170 and 0.9 h, h being total water depth).

171 2.1.2. Lacustrine environment

172 With volume of 1.8 – 58.3 billion m^3, the Tonle Sap lake is the largest freshwater source in
173 Southeast Asia (Kummu et al., 2014). It is located in the Cambodian floodplain (Fig. 1c) and
174 comprises a permanent waterbody, twelve tributaries, extensive floodplains and the Tonle Sap
175 river linking the lake to the Mekong river (Kummu et al., 2014). At the confluence, the river
176 splits into the Bassac river (Hau river) in the West and the Mekong river (Tien river) in the
177 East. The Tonle Sap system has strong and original hydrodynamic relationships with the
178 Mekong mainstream (Kummu et al., 2008). During the wet season, flooding from the Mekong
179 river causes a reverse flow direction, into the Tonle Sap lake. The lake area then increases
180 from 2500 km^2 to approximately 15000 km^2, while the depth rises from 1 to 9 m. At the
181 opposite, the slow release of floodwaters from the lake during the dry season is a very
182 important water source to sustain the river discharge of the Mekong delta (Hai et al., 2008). In
183 this specific paper, we focus on the physics of particles. The field survey was performed for 9
184 days from 13 October to 21 October 2018, during high flow season. The material used is
185 freshly deposited sediment, collected near the Mekong river tributaries, after a flood season at
186 the bottom layer.

187 2.1.3. Estuarine environment

188 The Mekong delta (MD) is situated at the most Southeast part of the LMR (Fig. 1d). It covers
189 approximately 55,000 km^2 (Balica et al., 2014), extending from the Cambodia - Vietnam
190 border to the Gulf of Thailand and the East Sea of Vietnam (Tran et al., 2018). Together with

191 the Mekong river and the Bassac river, it separates into eight tributaries (Hung et al., 2014)
192 before discharging into the East Sea (Wolanski et al., 1996 and Xing et al., 2017). At the
193 interface between land and the sea, the estuary is strongly impacted by both flooding from
194 upstream and the tidal flows, as well as wave forcing (Gugliotta et al., 2019).

195 Three surveys with contrasted seasonal conditions were conducted in the Song Hau estuary
196 (as part of the Lower Mekong Delta Coastal Zone project), in December 2015, March and
197 October 2016. During these surveys, three cross-sections (upstream - T1, middle - T2,
198 downstream - T3), with distances of 10 and 15 km, respectively, were chosen to monitor and
199 assess the impact of saline water intrusion on flocculation (Fig. 1d and sketch of Fig.6). At
200 each location, samples were taken in three vertical profiles. In total, 104 samples with volume
201 of 5 litres per sample were collected to investigate the spatio-temporal dynamics of suspended
202 sediment for contrasted sediment concentration (SSC) and turbulent levels.

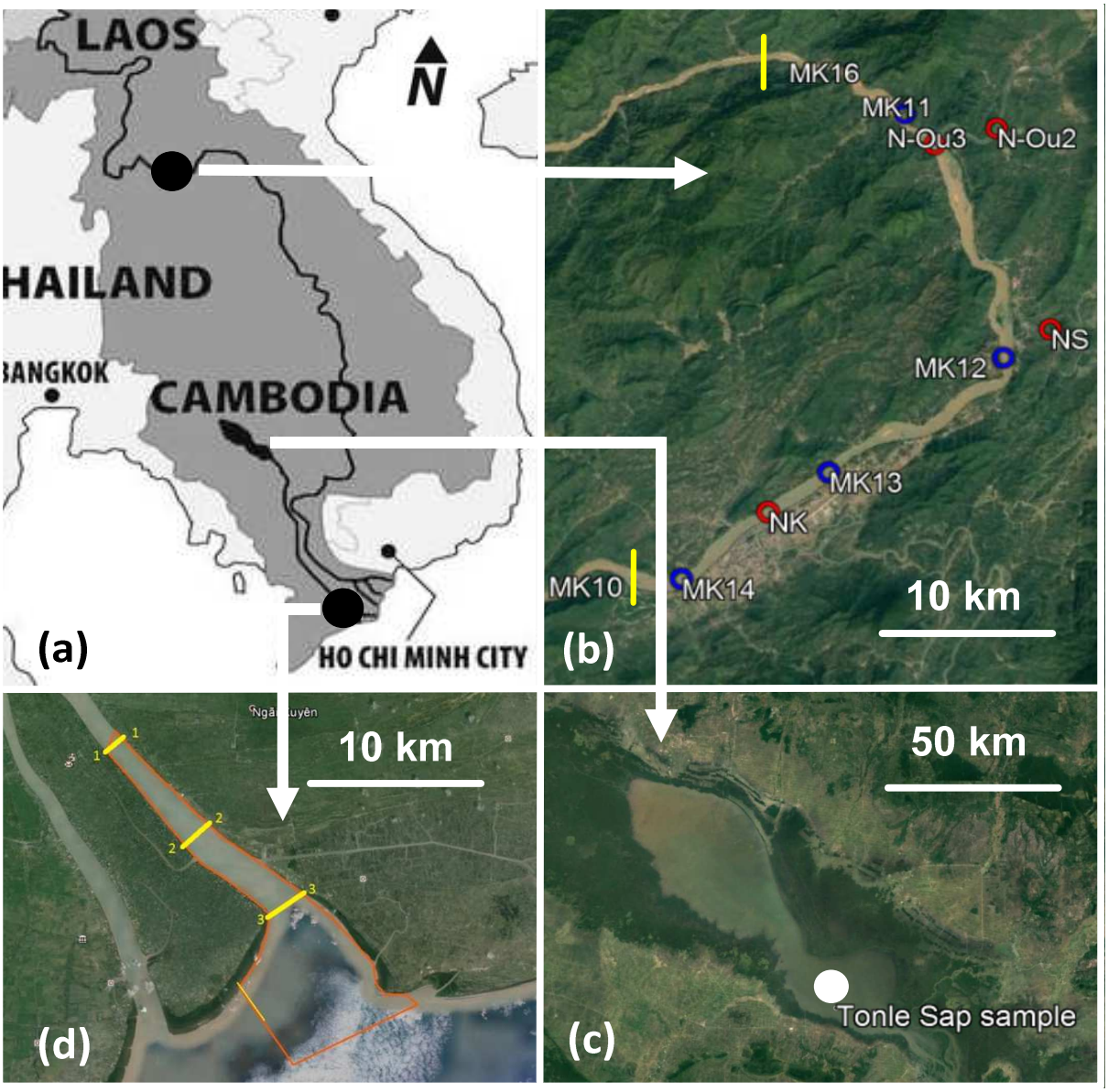

Fig. 1. Domains of interest [a] (Smardon et al., 2009). Sampling sites and locations in fluvial (Luang Prabang, Laos with blue dots reporting samples in main stream, red dots reporting samples in tributaries and yellow segments reporting cross-sections [b]), lacustrine environment (Tonle Sap floodplain, Cambodia with white dots showing the sampling location [c]), and estuarine environment (Song Hau estuary, Vietnam with yellow segments reporting cross-sections and red lines showing the local domain [d]).

2.2. Methods

The suspension regime of the sediments transported in a flow strongly depends on interactions between hydrodynamics, particle size, density and settling velocity. Thus, the understanding of particle size distribution (PSD) of suspended particulate matter (SPM) is one of prerequisites to properly simulate sediment dynamics (Fennessy et al., 1994). This study

originally proposes a direct estimation of settling velocity and flocculation with the patented SCAF instrument (System for the Characterization of Aggregates and Flocs, Gratiot et al. 2015).

The five sections hereinafter describe the methodology adopted to measure the physical properties of suspended sediment and evaluate its transport dynamics. The instruments at our disposal are particularly relevant to estimate both particle size and settling velocity, but it was not possible to measure directly the density of flocs, which may be seen as a limitation.

2.2.1. A portable mixing tank device to reproduce natural inflow turbulent conditions

To measure PSD under turbulent conditions close to the ones experienced by natural rivers, 2 litres of water samples were introduced into a portable rectangular-base mixing jar tank (with diameter of 11.5 x 11.5 x 15 cm), and then mixed with an impeller for thirty minutes. Since the work of Gratiot and Manning (2004), this mixing duration is assumed to ensure a good homogenization of the fluid mud mixture, and a dynamic equilibrium between the rate of flocculation and breakage. Some details on the experimental set-up can be found in Gratiot et al. (2017). During preliminary experiments, an Acoustic Doppler Velocity Profiler (Nortek Vectrino2) was immersed in the mixing tank filled with clear water, in order to measure the 3D turbulent field of velocity and deduce the mean turbulent energy dissipation rate G (s^{-1}). With a rotation speed of 100 rpm, G was about 44 s^{-1}, which corresponds to high shear rate conditions, such as observed near bottom in natural rivers and estuaries (Gratiot et al., 2017). For further details on the mixing tank device, the reader can refer to Gratiot et al. (2017, supplementary information).

2.2.2. PSD measurements and characterization of the particle-classes/population/group?

To characterize the different populations of particles, the terminology of Lee et al. (2012) is used. It is based on four classes, namely primary particles, flocculi, microflocs and macroflocs (as mentioned in the Introduction section). We utilize the LISST-Portable XR instrument to measure sediment particle sizes during mixing. The operational principle of the LISST-Portable XR is based on laser light scattering (or laser diffraction). This instrument provides the logarithmical PSDs over 44-size bands in the ranges of particle size from 0.35 to 500 µm by using the Fraunhofer approximation or the exact Lorenz-Mie theory. The volumic concentration is in micro-litre/litre ($\mu L.L^{-1}$), corresponding to sediment concentration of 30 - 1900 $mg.L^{-1}$ in the chamber of measurement. Each spectrum shows independent semi-log distributions of sub-populations, that were characterized by their mean particle size D_f, their

247 standard deviation σ_{Df} and their relative volumetric concentration. The operating range of
248 optical transmission recommended by LISST-Portable XR is 75 - 95 %. For optical
249 transmission lower than 75 %, multiple-scattering can bias the signal and lead to an
250 underestimation of the size distribution.
251 This device has been utilized successfully in many contrasted environments, such as the
252 Saigon - Dong Nai rivers, Vietnam (Nguyen et al., 2019), a hydropower plant in Malaysia
253 (Azrulhisham et al., 2018), Northern French Alps (Antoine et al., 2015) and Philadelphia
254 (Windt et al., 2017), among others.
255 It is worth noting that many other techniques exist to measure PSD, particularly video-based
256 techniques, such as the immersed INSSEV instrument (Fennessy et al., 1994) or the LabFlocs
257 portable video system (Manning et al., 2007). All methods have advantages and
258 disadvantages, so that a combination of different techniques is probably the best efficient.
259
260 For describing PSDs of primary particles, flocculi, microflocs and macroflocs, we apply a
261 mathematical function to separate the signal into four log-normal distribution (Mikkelsen et
262 al., 2006). Such post processing is also useful to prevent misinterpretation, resulting from air
263 bubbles and other artefacts that can be observed in the raw particle size spectrum (Sequioa,
264 2016).
265 In this study, the PSD of each sample was measured in two steps, before and after two
266 minutes of sonication, for a mechanical particle breakage under acoustic waves. Hence, it is
267 possible to assess the proportion of sand and flocs because large-size particles built by smaller
268 cohesive particles (silt or clay) are, at least partially, dispersed by sonication (Gratiot et al.,
269 2017) while the sand particles are indivisible and then maintain a constant diameter after
270 sonication.

271 2.2.3. Characterization of the settling and flocculation regimes

272 Depending on SSC, three settling regimes can be observed for natural sediment in aquatic
273 environment (Van Leussen, 1994), namely (1) free settling, (2) flocculation and (3) hindered
274 regimes. For the lowest SSC, flocculation is weak and particles are settling almost
275 independently from each other (free settling regime). Particle settling velocity can then be
276 broadly estimated by the Stokes' law or derived laws as the sum of individual particles
277 settling down (Stokes, 1857; Winterwerp, 2002). The flocculation settling regime occurs with
278 midrange of SSC (tens to hundreds of $mg.L^{-1}$). The settling velocity of cohesive and mixed
279 fine-grained sediments then becomes more complex because it is influenced by both particle

interactions and individual properties (Manning et al., 2010), as well as turbulent shear (Winterwerp, 2002; Manning et al, 2011a). Flocculation is promoted, which results in larger particle sizes and higher settling velocities (Droppo et al., 2005). The hindered settling regime occurs at very high SSC (several grams per litre or more), and settling mostly occurs by mass, depending on the cohesion and suspension concentration (Camenen and Van Bang, 2011; Van and Van Bang, 2013).

To assess the settling velocity w_s ($m.s^{-1}$) (and flocculation) for all these regimes in natural environment, we used the System for the Characterization of Aggregates and Flocs (SCAF), a recently patented instrument (Gratiot et al., 2015) that was successfully applied in some recent researches (Wendling et al., 2015, Gratiot et al., 2017, Legout et al., 2018, Nguyen et al., 2019). This instrument is a glass settling column with dimension of 20 cm high and 3.5 cm in diameter, equipped with 16 infrared (λ = 980 nm) emitters and 16 diametrically opposed photo-sensors measuring at a frequency of 210 Hz. SCAF instrument measures the light attenuation in the settling tube with depth and time during the deposition of particles (Gratiot et al., 2015). Sensors are located every 1 cm down the column with the lower sensor located at 1 cm above the bottom of the column. Measurements taken in the eight upper centimeters of the SCAF settling tube provided an estimate of flocs settling velocity under quiescent conditions, denoted $w_{s,q}$ ($m.s^{-1}$) while measurements realized in the eight centimetres near the bottom of the settling tube provided an estimation of flocs settling velocity after flocculation by differential settling under settling dominated conditions, this latter velocity being reported as $w_{s,\neq}$ (Wendling et al., 2015). In the case of non-cohesive particles, such as sand or silt, or clay particles with deflocculant, the settling velocity does not change during settling; $w_{s,q}$ and $w_{s,\neq}$ are similar and the flocculation index FI = ($w_{s,\neq}$ - $w_{s,q}$)/ $w_{s,q}$ is close to zero (Wendling et al., 2015). As SCAF instrument is based on by mass sedimentation of a fluid mud mixture in a settling tube, it is inherently affected by the shape, density and compositions of all particles presented in the sample.

2.2.4. Other hydrodynamic measurements

Complementary measurements were performed during field surveys. An Acoustic Doppler Current Profiler (ADCP), an Hydrolab probe (a multi-parameter probe measuring in-situ water quality parameters), SSC samplers and a EUTECH turbidimeter were used to characterize the water flow in the cross-sections, suspended solid concentration and physical parameters such as turbidity, temperature, pH, ORD, EC, salinity, etc. An YSI multi-

parameter probe (Water Quality Sampling and Monitoring Meters and Instruments) was also used to check the average values of the measured physical parameters.

2.2.5 Characterization of the suspension regime

In order to characterize the suspension regime, the non-dimensional Rouse number (Rouse, 1937), which express the balance between the upward turbulence forces (u_*) lifting the particles and the gravity forces applied (W_S) on the same particles in a river stream, was calculated for each flow condition encountered. The Rouse number is calculated as following:

$$R_o = \frac{w_S}{\beta \kappa u_*} \quad (1)$$

where the settling velocity w_s is inferred from the SCAF results (Fig. 5), or calculated by the Stokes' Law from the PSD measurements. κ is the von Kármán constant, taken equal to 0.41. The constant of proportionality β is the ratio of sediment to eddy diffusivity, describing the diffusion patterns of a fluid particle and a sediment particle. In water environment, it is often assumed that eddy viscosity is equal to eddy diffusivity, thus value β is typically hypothesised to be one (Rijn, 1984; Farrell and Sherman, 2013). u_* (m.s^{-1}) is shear velocity. In the fluvial and estuarine environments, the shear velocity u_* was computed by using the ADCP, with the assumption that the velocity profiles follow the logarithmic inner-law (so-called "Law of the Wall") (Sime et al., 2007; Santini et al., 2019, Eidam et al., 2017). In the lacustrine environment, u_* was computed from 2D hydrodynamic simulation results by the Second-generation Louvain-la-Neuve Ice-ocean Model (SLIM, https://www.slim-ocean.be/).

The application of Eq.1 to characterize the suspension regime is relevant, but we should underline that uncertainties can be high, as both W_S and u_* are hardly estimate in the field.

3. Results

3.1. Particle size distribution (PSD)

The PSD of all samples are gathered in a triangle sketch in Fig. 2. Before sonication, most of the particles are flocculi with an average contribution percentage of 46 %, 78 % and 78 %, for fluvial, lacustrine and estuarine environments, respectively (Fig. 2a). After sonication, the PSD displayed an increased number of primary particle class for all samples (51 %, 67 % and

32 %, respectively), while it witnessed the reduction in the percentage of flocculi and flocs (Fig. 2b). This figure also shows a wider diversity of particle sizes in the Mekong estuary (blue circles and squares) than in the lacustrine and the fluvial environments (yellow and red circles, respectively). It illustrates that estuaries are complex and changing environments, which mix both fluvial and coastal water (see the sketch in Fig.6 and the corresponding discussion section). In the case of the Mekong estuaries zone, sediment transport and deposition is strongly affected by fluvial inflow, tidal currents, but also resuspension of particles by wind-induced current, waves and coastal oceanic currents (Gugliotta et al., 2019; Marchesiello et al., 2019).

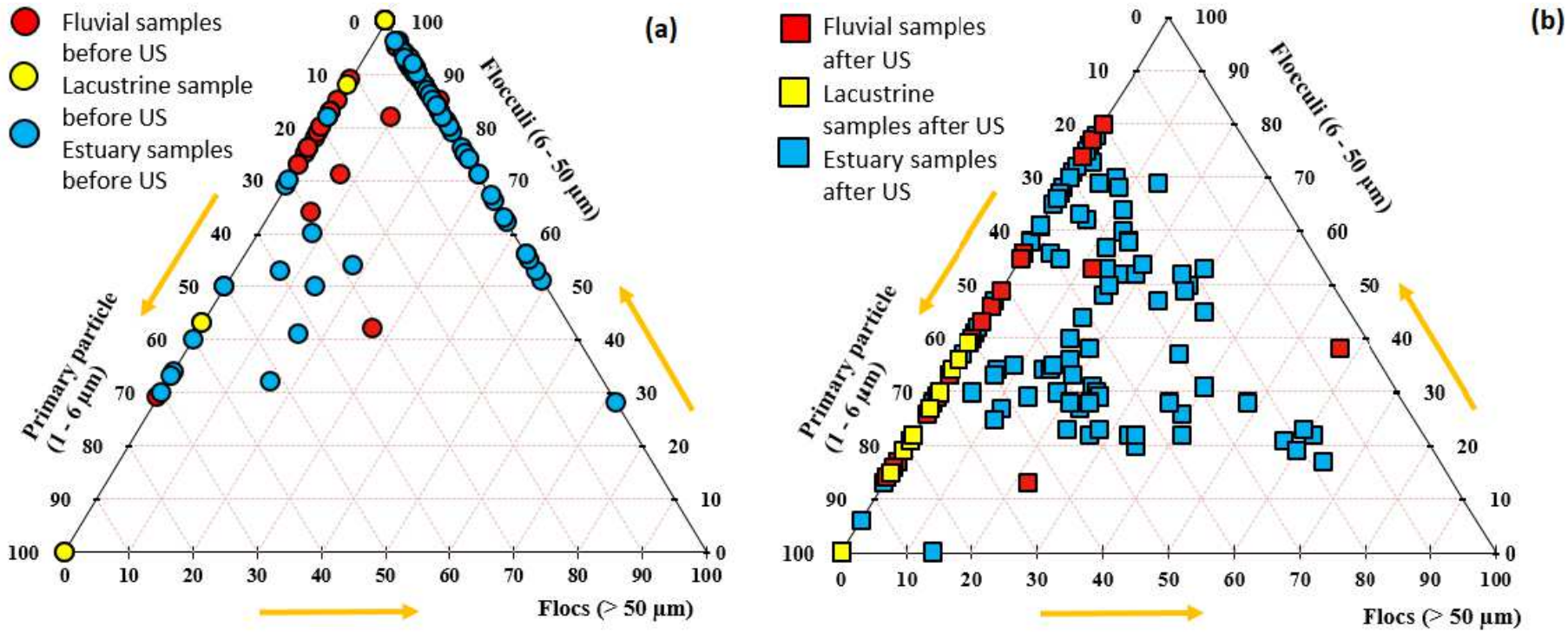

Fig. 2. Triangulars of PSD in upper parts and estuary analyzed (a) before and (b) after sonication

350 *3.2. Suspended sediment versus hydrodynamic conditions*

351 Fig. 3 aims at highlighting the role played by SSC on flocculation of particles. This figure
352 gathers both data collected in the field and in the laboratory, before and after sonication.

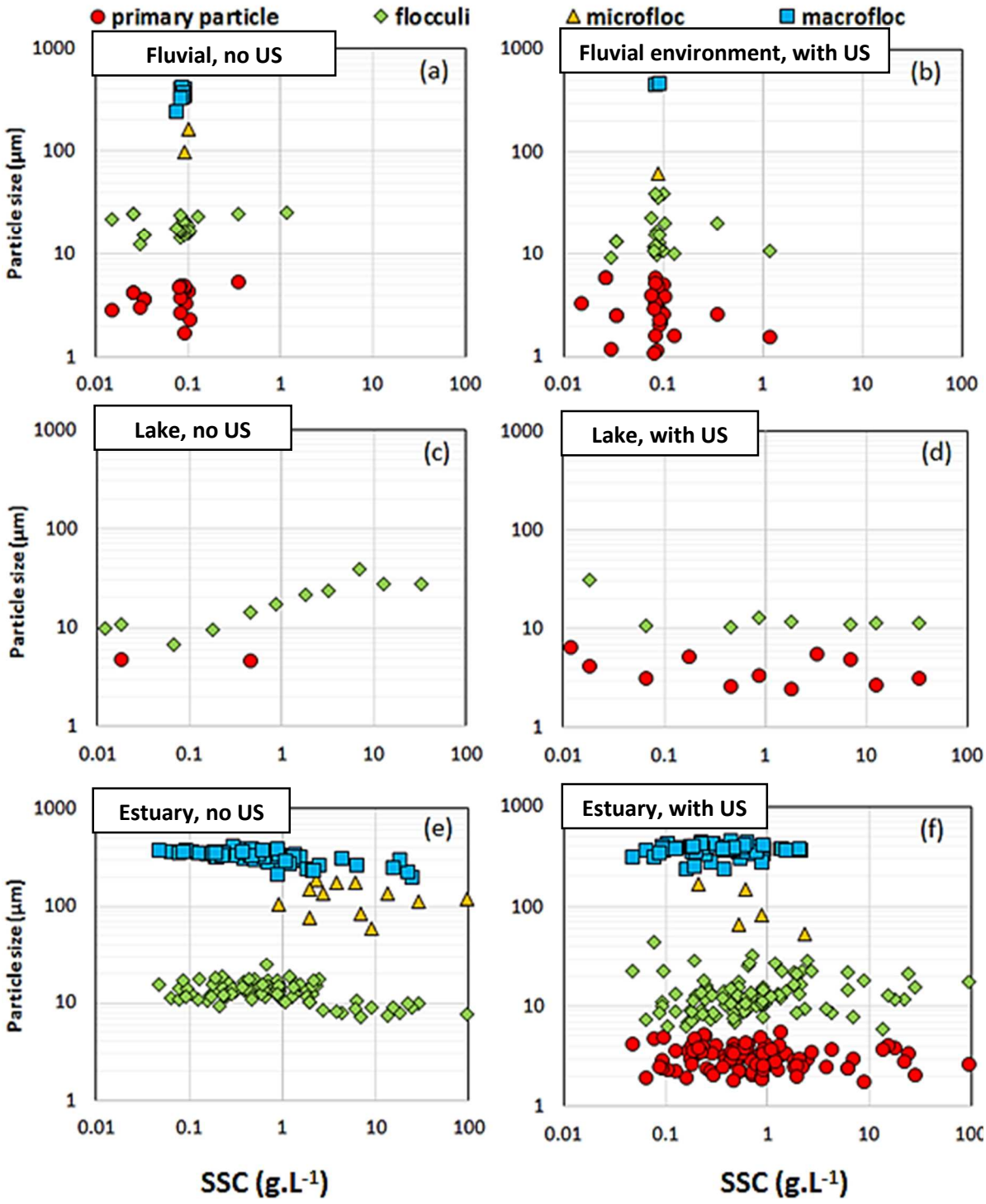

353

354 **Fig. 3**. Variation of particle classes with SSC in fluvial environment, lacustrine environment
355 and estuary before and after sonication

356 3.2.1. Particle size populations in the fluvial environment (Laos)

357 Fig. 3 (a) and Fig. 3 (b) present the PSD of particles populations sampled in the fluvial
358 section. On average, the primary particles accounted for 37 % of all particle population (in
359 volumetric concentration). The predominant population is flocculi, with a volume
360 concentration of approximately 46 %. Microflocs and macroflocs were fewer and accounted
361 for (only) 3 % and 14 % of the total volume, respectively. The macroflocs size reached a
362 median diameter of 422 µm. Fig. 3 (b) shows the PSD plot after sonication. The sonication
363 broke up particles so that the percentage of primary particles increased (+14 %) to 51 % and
364 flocculi decreased slightly (-5 %) to 41 %. The percentage of microflocs remains stable and
365 small (approximately 2 %), and the percentage of macroflocs decreases by more than two
366 folds (to approximately 6 %). These coarsest particles were not all broken up by sonication,
367 which indicates the presence of sand. The samples issued from the tributaries had generally
368 similar PSDs than the ones in the mainstream. After sonication, PSD of these samples still
369 exhibits high values, with a maximum diameter of 347 µm. It means that these water samples
370 contains predominantly sand, which is in agreement with visual observations during field
371 campaigns. A detailed examination of PSD before and after sonication confirmed that samples
372 in fluvial environment consisted of both cohesive sediment and sand particles. These PSDs
373 are in agreement with the results of Camenen et al. (2014).

374 3.2.2. Particle size populations in the lacustrine environment (Tonle Sap, Cambodia)

375 In the lacustrine environment, only two particles classes (primary particles and flocculi,
376 without flocs and no sands) appear. Before sonication (see Fig. 3c), the percentage of primary
377 particles and flocculi accounts for 22 % and 78 %, respectively. After sonication (see Fig. 3d),
378 these percentages reverse with a predominance of primary particle (67 %) and a simultaneous
379 decrease of flocculi (33 %). The particle size in the lacustrine environment were smaller (7 ±
380 3 µm) than in the fluvial part (18 ± 5 µm). Fig. 3c exhibits a clear rise (3 to 4 folds) of flocculi
381 size with higher SSC, as a response of flocculation of primary particles (or colloids) on
382 flocculi.

383 Interestingly, colloids were observed in some samples taken in the Tonle Sap, with diameters
384 of < 1 µm (see Fig 4). After 12 hours of deposition in the mixing tank at rest, the particles still
385 in suspension were both colloids with diameter of approximately 0.45 µm, which are
386 consistence with a research conducted by Seah et al 2017, accounting for 21 %; primary

particle (73 %) and few flocculi (6 %). After sonication, the structure of sediments presents the same pattern (21 % of colloid, 72 % of primary particles and 7 % of flocculi). This can be explained by a stable mixture of this sediment classes, which are hardly broken down into smaller particles even after sonication. Colloids play an important role and act as "catalyzers" of the interaction between sediment and substances in the water such as substance dissolved matter, substance from precipitation, absorbed ions and organic matters (Wendling et al., 2015).

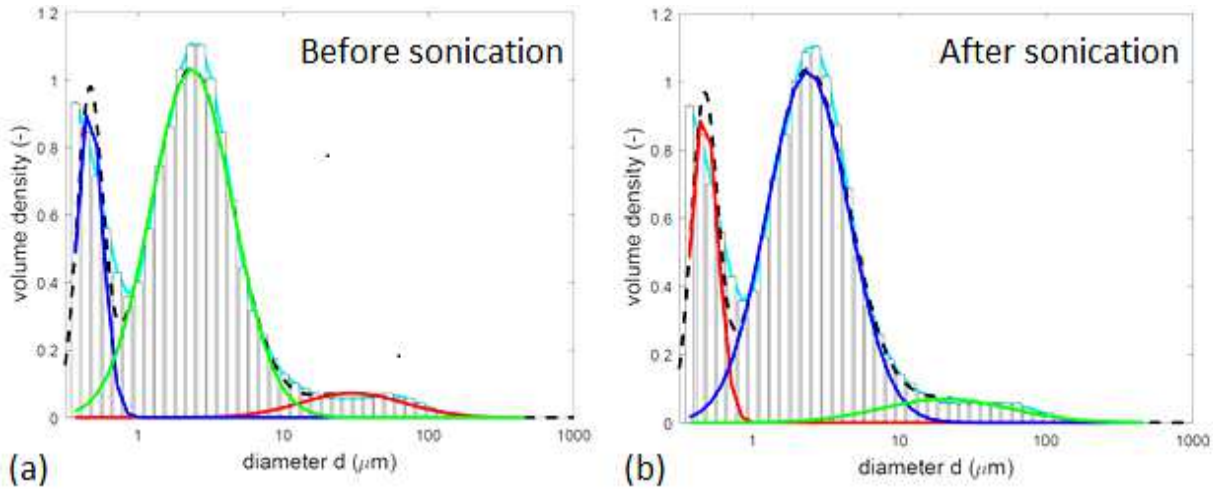

Fig 4. PSD of a sample in the Tonle Sap before (a) and after sonication (b). The first peaks in two graphs show the appearance of colloids with diameter of < 1 µm.

3.2.3. Particle size populations in the estuarine environment (Song Hau river, Vietnam)

Fig 3 (e and f) display the PSD in the estuary versus SSC before and after sonication, respectively. Once again, flocculi is the dominant population of particles, with mean diameter of approximately 15 µm (in range of 8 - 20 µm), accounting for 80 % of total volume. Before sonication, only three classes of particle sizes exist in the estuarine samples, flocculi, microflocs and macroflocs. The prevailing fine silt population shows mean diameter of 7 – 12.5 ± 10 % µm, that constituted 83 – 94 % of total volume. Diameters of coarser population were in the range of 112 – 310 ± 10 % µm. After sonication, particle size reduced significantly. A group of primary particles (red circles), which were completely absent from the PSDs before sonication, appears in almost all samples, which undoubtedly demonstrates the cohesive nature of sediments in the estuary. Due to breakage into smaller particles under turbulence shear, diameters of fine particles (primary particles and flocculi) reduce to 1.8 – 4 ± 10 % µm and 6.3 – 12.2 ± 10 % µm, respectively while the size of coarse particle

(microflocs) falls to 15 – 65 ± 10 % µm. A population of sand particles (with diameter > 200 µm), not broken-up with/after sonication, is also evidenced.

3.3. Settling velocity

Fig. 5(a) shows the variation of suspended sediment settling velocity with SSC, measured directly with SCAF instrument. For the three aquatic environments, settling velocity rises with SSC because of flocculation process. Even if there are only 5 SCAF samples in the fluvial environment, 9 samples in lacustrine environment, 19 samples in the estuary, the three curves exhibit similar trends, which support the existence of free settling, flocculation and hindered regimes, as previously depicted by Wendling et al. (2015).

The free settling regime is observed for the lowest SSC (tens of $mg.L^{-1}$). Sediment settling velocity measured in the fluvial, lacustrine and estuarine environments are of the same order of magnitude, the mean settling velocities being approximately 0.02 - 0.08 $mm.s^{-1}$ in the fluvial section, 0.05 – 0.06 $mm.s^{-1}$ in the lake, and 0.01 - 0.02 $mm.s^{-1}$ in the estuary. The widest range of settling velocities observed in the fluvial environment is probably the fingerprinting of a wide variety of compact soil aggregates, freshly eroded from the watershed, and not yet at equilibrium with the prevailing hydrodynamic conditions, as reported conceptually by Droppo et al. (2015). In this free settling regime, particles settle almost independently, the interaction between particles is poor, which is reflected by a moderate flocculation index (FI lower than 2) in all SCAF measurements (in Fig. 5, right panel). Flocculation predominates in the range of 0.4 - 4 $g.L^{-1}$, thus the settling velocities of fluvial, lacustrine and estuarine sediments rise up to 0.2 mm s^{-1}, 0.1 – 2 $mm.s^{-1}$ and 0.03 – 0.8 $mm.s^{-1}$, respectively.

In the lacustrine environment, a significant rise of settling velocity is found with higher SSC. The SCAF results show that the settling velocity of the lacustrine environment reaches the peak of 2.0 $mm.s^{-1}$ when SSC reach approximately 2.0 $g.L^{-1}$.

In the estuary, the complex hydraulic regimes, including resuspension of freshly deposited sediments (Marchesiello et al., 2019) and the mixing between fresh water and saline water led to the formation of a zone of turbidity maximum and promote the formation of flocs (both microflocs and macroflocs) (Dyer et al., 2002a and Manning et al., 2007). As a consequence, the settling velocity also increases (Dyer et al., 2002b and Manning et al., 2011b). Beyond 4.0 $g.L^{-1}$, hindered regime becomes predominant. It implies the decline of settling velocity in the

441 lacustrine and estuarine environments, from 2.0 to 0.4 mm.s^{-1} and from 0.8 to 0.1 mm.s^{-1},
442 respectively.

443 The main difference of these three environments is that flocculation processes seem to appear
444 at lower concentration in the fluvial environment (approximately 20 - 30 mg.L^{-1}) than in the
445 lake (approximately 1 - 2 g.L^{-1}) or in the estuary (approximately 300 mg.L^{-1}). We cannot
446 exclude that the particles sampled in the fluvial environment are not real flocs, but correspond
447 to soil aggregates that are not in equilibrium with their hydraulic environment (Droppo et al.,
448 2005).

449 The flocculation efficiency is higher for the estuarine environment (+ 60 % of increase of the
450 settling velocity) and highest for lacustrine environment (+200 % of increase) than for the
451 fluvial environment (+7 % of increase).

452 Concerning the Flocculation Index (FI), sediment samples in the river and in the lake (red
453 circles for fluvial environment and yellow circles in lacustrine environment, see Fig. 5b)
454 exhibit a high dynamic, even in fresh water. The highest rate of flocculation is observed in the
455 lacustrine environment, where the measured FI increases from 0 to 6, when SSC increases
456 from 0.1 to 3.0 g.L^{-1}. Interestingly, after getting the FI peak of 4 – 6, the efficiency of
457 flocculation in the lacustrine environment fell to value of 0 – 1.75. It means that flocculation
458 still occurs, but the volumetric concentration of particles is so high that the settling velocity
459 cannot increase anymore. Settling velocity of small particles is hindered by the high SSC,
460 whereas colloids are trapped on the surface of larger particles (Comba et al., 2009).

461 The estuarine sediments also experience three settling regimes with FI in range of 0 - 3: (1)
462 Free settling regime with constant FI of 2, that is developed at low concentration of 300 mg.L^{-1};
463 (2) Flocculation regime with FI < 3, where flocculation happens at SSC of 300 - 2700 mg.L^{-1};
464 and (3) Hindered regime with FI of approximately 1 because of the appearance of brackish
465 water and high SSC of > 2.7 g.L^{-1}. Flocs reach higher volumetric concentration for lower
466 mass concentrations when flocculation is reinforced by differential settling (Gratiot et al.,
467 2017).

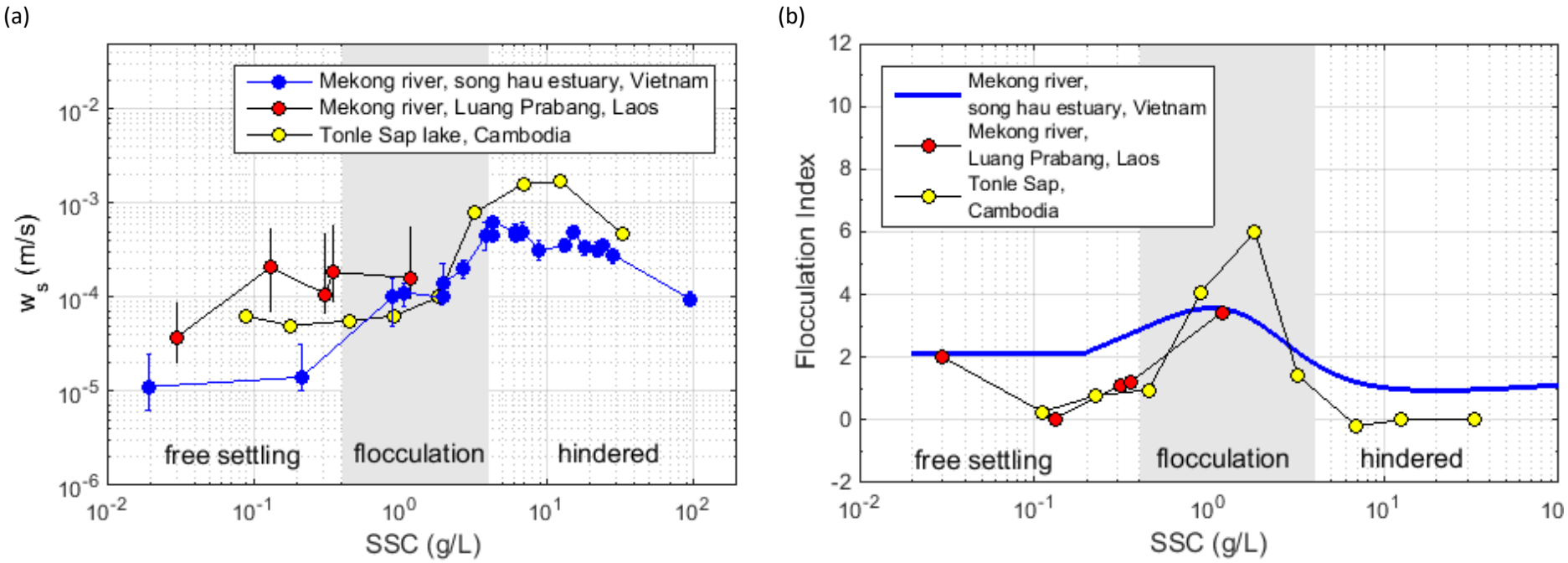

468 **Fig. 5.** Sediment properties in the Mekong Land to Ocean Continuum: (a) Variation of settling velocity with SSC measured directly with SCAF
469 instrument and (b) Variation of the flocculation index with SSC.

4. Discussion

4.1. Suspended sediment transport mechanisms along the Mekong

As mentioned in Section 2.2.4, the transport regime of suspended sediment along the LMR may be characterized through the non-dimensional Rouse number (R_o). For the upstream fluvial environment, the computed shear velocities were similar in the different sections monitored, u_* = 0.03 m.s^{-1} for the MK10 and u_* = 0.04 m.s^{-1} for MK16. The small difference between the two cross-sections may be explained by the geometry of each cross-section, MK10 cross-section being wider than MK16 cross-section. The shear velocity in the Tonle Sap is 0.008 m.s^{-1} by using SLIM simulation obtained by Le et al. (submitted); while a value of 0.010 m.s^{-1} is obtained by using the Inner law. The R_o values in the estuary are estimated based on two representative particle sizes (15 µm for fine particles and 300 µm for sand) and the shear velocity is estimated with the recent work of Eidam et al. (2017).

The R_o values estimated for the fluvial, lacustrine and estuary environments are summarized in Table 1. In the fluvial environment, the R_o ranges between 0.002 and 0.009 at the two monitored river cross section (MK10 and MK16), which corresponds to the washload mode. Hence particles are presumably transported over long distances, without any interaction with the riverbed. Few sand particles are presents in the MK10 and MK16 cross section samples, with R_o values of 0.75 - 4.6. Its means that the very fine sand particles are strongly sorted over the water depth, leading to a low suspension mode. As for the coarser sand fraction of the riverbed, the stream was not able to transport them in suspension.

While R_o values of Tonle Sap samples vary from 0.005 – 0.015, corresponding to flow modes ranging from washload to strong suspension load (Vanoni et al., 1946 and Udo et al., 2011). It is assumed that sediments are deposited near bed during one part of the year, and eroded under wind-induced currents during another part of the year. According to Kummu (2008), the net budget of sediment is almost in equilibrium between deposition and erosion.

In the estuary, the value of the R_o for the fine sediments ranges between 0.007 - 0.058, which corresponds to strong suspension mode; while the values for sand vary from 2.4 to approximately 12, which corresponds to the bedload mode and sedimentation dominated regime (Gugliotta et al., 2019). This finding coincides with the recent study of Marchesiello et al. (2019) showing that the Mekong sediments consist of a mixture (fine sediments and sands)

under effects of complex forces. Thus coastal muds are exposed to wave-induced resuspension and wind-induced transport, while sands are concentrated near the estuaries.

Table 1. Ro value in two different conditions

Sample	Mean Diameter (μm)	u_* (m.s^{-1})		w_s (m.s^{-})		Rouse value	
		Law of Wall	Modelled results	SCAF	Stokes' Law	Min	Max
Fluvial (MK10)	19 ± 2	0.029	-	2.0E-05	1.2E-04	0.002	0.009
Fluvial (MK16)	18 ± 4	0.041	-	8.0E-05	1.2E-04	0.005	0.007
Tonle Sap	7 ± 2	0.014	0.008	5.0E-05	2.0E-05	0.005	0.015
Estuary fine sediment	15 ± 2	-	0.01	3.0E-05	2.4E-04	0.007	0.058
Estuary sand	300 ± 30	-	0.02	2.0E-02	9.5E-02	2.439	11.6

4.2 Predominance of flocculi in the LMR and consequences for sediment transport

As quantified in this paper, flocculi is the dominant particles population in all three environments monitored at regional scale (46 % in the fluvial environment, 78 % in the lake and 78 % in the estuary). The existence of sand was noticed, but can mostly be found near the bed with few percent of volume.

In the Lower Mekong River as in many other large hydrosystems under tropical climates, we may anticipate that particles' populations (and its consequences) fluctuate seasonally and year after year. As designed, this study cannot catch these variations, however, we believe that it describes a general pattern that could be helpful when establishing some monitoring strategies in similar large tropical hydrosystems in South East Asia, and probably elsewhere. At large scale, Rouse analysis presented in Table 1 showed that particles are mainly transported with a strong suspension regime, evenly as washload by river flow. By these modes, they are transported abundantly along the main river and tributaries, partially over the floodplains during the flood season (Kondolf et al., 2014, Manh et al., 2014, Manh et al., 2015) and then, are deposited along shore and on the whole subaqueous delta, before having cycles of resuspension/deposition, principally under waves forcing (Marchesiello et al., 2019). Our measurements in the fluvial section show that few sands are transported in the water column because their transport, which do not flocculate, is completely governed by the stream power. During high flow with enhanced stream powers working with other sediment sources (riverbanks and floodplains), the finest sands are lifted into upper layer.

This methodology can explain two distinct transport modes of two particles populations in the Mekong estuary: washload is well mixed throughout the water column and sand are transported prevailing near the bottom. It leads to distinct geomorphological forms, with the presence of alternated tidal flats and sand bars as observed in many river mouths (Ta et al., 2002; Gupta et al., 2002; Anthony, 2015).

4.3. Occurrence of fluid mud layers in the Mekong estuary

According to measured data during our three surveys in the estuary, a fluid mud layer was sometimes formed near bottom, with SSC values abruptly increasing beyond 0.4 $g.L^{-1}$, corresponding to the transition to the flocculation regime (Fig. 5; Gratiot et al., 2017). Fig. 6 sketches the sediment transport from the river to the estuary in low flow season (a) and high flow season (b) with locations of vertical profile sampling. In this figure, the blue profile represents a schematic profile measured in low flow season and the purple one represents a profile measured in high flow season. Fig. 7 reports all SSC value observed near bottom ($z = 0.9h - SSC_{nb}$) for the vertical profiles realized in the estuary in December 2015 (50 profiles), March 2016 (44 profiles) and October 2016 (47 profiles). Each vertical profile is represented by a single point in Fig. 7. The three curves show the sorted distribution of all SSC_{nb} values for the three seasons. The curves show that the percentage of profiles which exhibits high SSC values, compatible with fluid mud layer occurrence, is very high during low flow season (66 % of profiles in Dec 2015 and 95 % profiles in March 2016) and is much smaller during high flow season (9 % profiles in October 2016).

By multiplying SSC_{nb} values with the corresponding settling velocity w_s reported in Fig. 5, we can estimate the settling flux capacity of fluid mud layers $\phi = SSC_{nb} \times w_s$ and thus assess their potential contribution to sedimentation (Fig. 7b). The cumulated sorted series demonstrate the strong linearity between sediment concentration and settling flux (i.e. potential of sedimentation). Fig.7c shows that the 10 % of the most concentrated fluid mud layers contributes to 60 % of the sedimentation during low flow season (blue curves) and more than 98 % during high flow season (purple curve).

As a preliminary conclusion, our study confirms the existence of fluid mud layers and quantifies broadly their frequency of occurrence in the estuary. Fluid mud layers are observed within distances of approximately 30 km from the coastlines in both high flow and low flow seasons. However according to Wolanski et al. (1998), the location of fluid mud layer in the

Mekong estuary varies spatialy with river discharges and tides. In the high flow season, most of sediment deposits in shallow coastal waters, approximately 10 - 20 km from the coast (Wolanski et al., 1998 and Marchesiello et al., 2019). In low flow season, fine sediment is well mixed with saline water penetrating about 40 km inland, carrying sediment up-river to a turbidity maximum zone. Further upstream, at Can Tho, approximately 120 km from the coast, no turbidity maximum is found in the freshwater region of the estuary. Thus the positions of fluid mud layers and turbidity maximum, which are promoted by SSC concentration in the range 0.4 - 4 $g.L^{-1}$, can hardly be observed for distances higher than 120 km inland. This situation could change in the future, under the cumulated effect of subsidence and sea level rise.

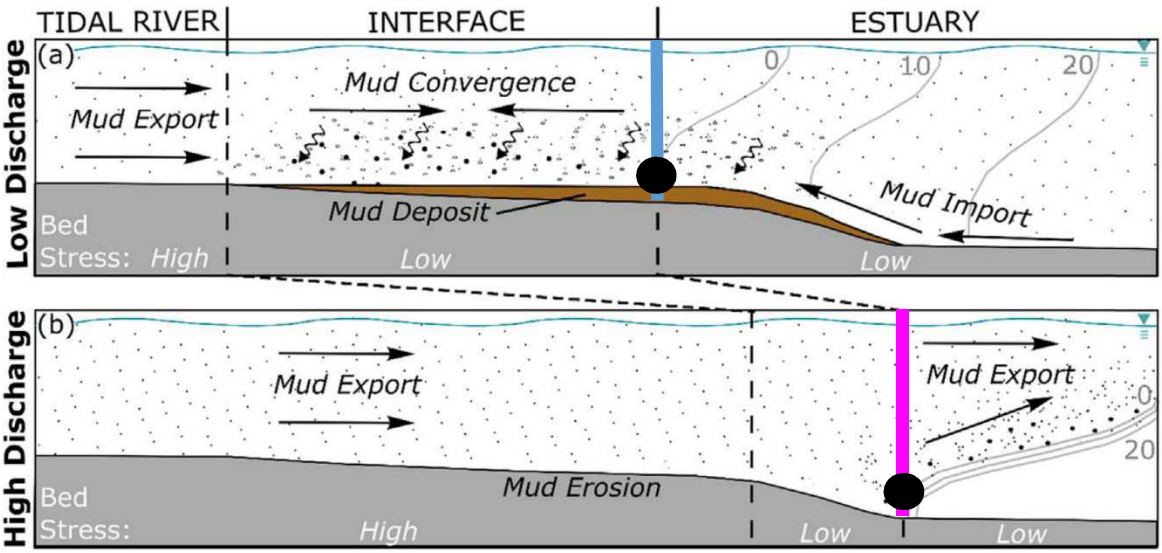

Fig 6. Conceptual summary of salinity stratification (grey lines), SSC (dot concentration), relative near-bed shear stress, suspended particle aggregation (dot size), net sediment advection (black arrows), and mud deposition/erosion within the tidal river, tidal river – estuary interface, and estuary during (a) low and (b) high discharge seasons. Relative weight of transport arrows vary with season and regime. Not drawn to scale (after McLachlan et al., 2017). The blue line shows the vertical profile in low flow season and the purple line shows one in high flow season with SSC. The black dot shows the sampling height (near bottom, at 0.9 h).

According to Spearman and Manning (2008), the mass balance between accretion and erosion of cohesive sediment during tidal cycles in estuarial location can occur when threshold shear stresses for both deposition and erosion operate simultaneously.

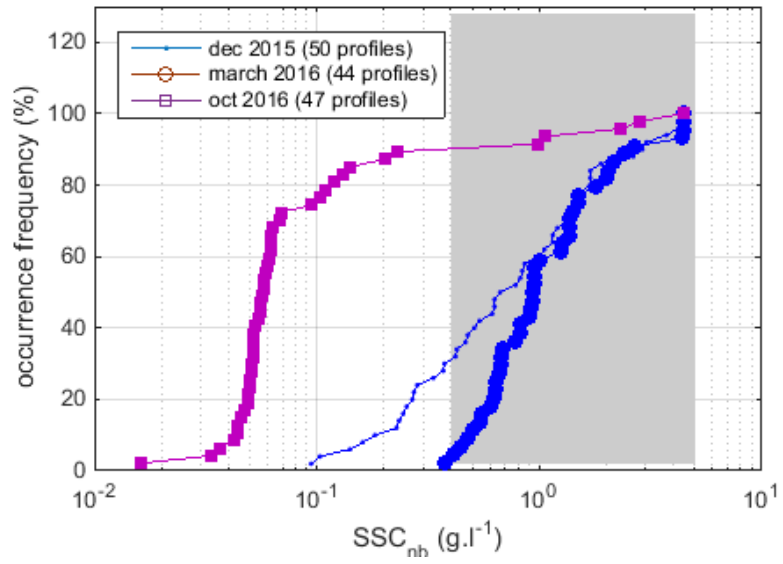

(a)

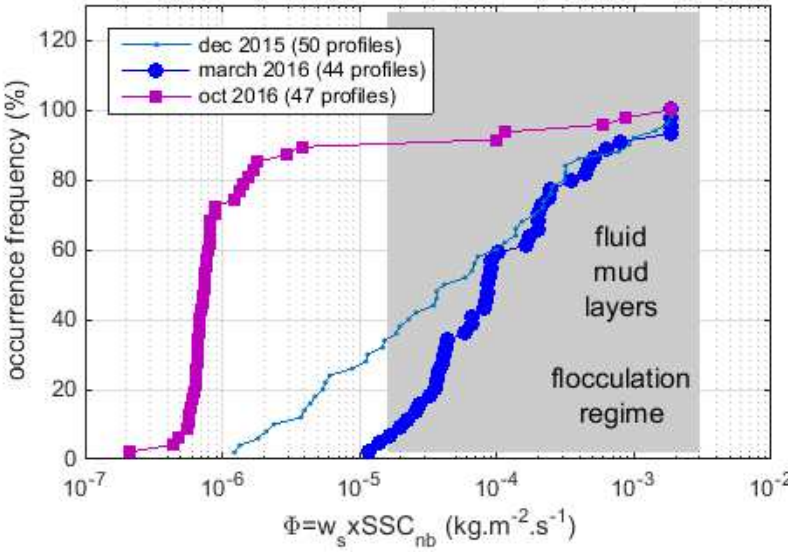

(b)

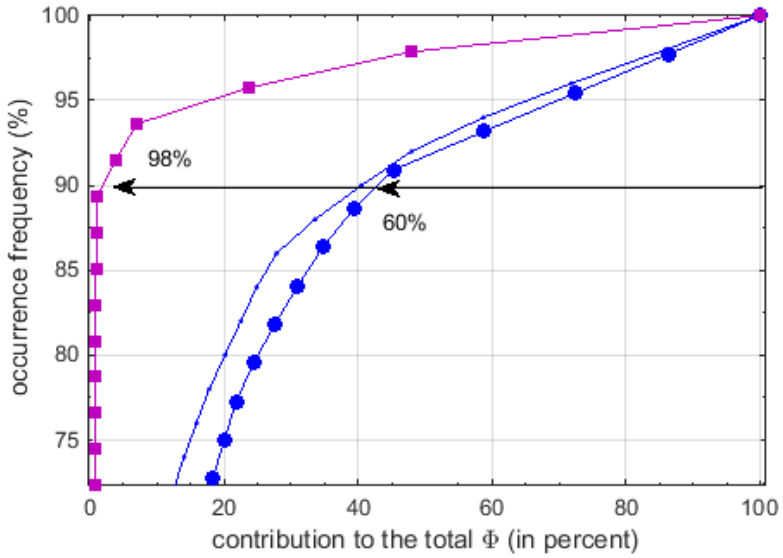

(c)

Fig 7. Data corresponds to SSC measured near bottom ($SSCn_b$). Data are sorted from lowest to highest SSC (a), corresponding settling flux (b) and contribution to the total (c). The blue line shows the vertical profile in December 2015; the blue line with dots shows one in March 2016 and the purple line shows one in October 2016 with SSC near bed.

576 *4.4. Implication for Mekong Delta management*

577 In the MD, the flocculation process plays an essential role in the formation of fluid mud layer
578 by enhancing the downward flux of sediment when freshwater mixes with seawater and
579 sediments become trapped at the convergence point. Sediments leaving the MD appears to go
580 through cycles of trapping and resuspension in the estuary, before being partially advected
581 seaward on the subaqueous delta and alongshelf, where they are largely incorporated into
582 fluid mud along the bottom salinity front. The fluid muds have far-reaching effects on the
583 coasts by reducing boundary shear stresses, attenuating of waves over a soft muddy bottom,
584 affecting water-column /seabed exchanges, and serving as the agent of outward growth of the
585 subaqueous delta (Marchesiello et al., 2019). In addition, fluid mud layers can lead to rise in
586 fluid viscocity and density, and the reduction of bottom shear stresses can affect on the tidal
587 wave propagation (Gabioux et al., 2005). Thus without flocculation, the particles would be
588 carried directly offshore (Kineke et al., 1996). The appearance of fluid mud layer under
589 flocculation regime provides a mechanism for rapid and strong sedimentation in the estuaries
590 and lead to local siltation and mud accretion. Once deposited in the bed, fluid mud layers
591 contribute to bedform development and stability (Schindler et al., 2015). We should underline
592 that bedform consolidation and stablility is hardly predictable, because it depends on both
593 physical and biological near bed processes (Parson et al., 2016) that evolve continuously for
594 sediment mixtures containing cohesive mud and biologically active substances such as
595 microorganisms, bacteria and microphytobenthos who form biofilms (Malarkey et al., 2015).

596 How can we anticipate the impact of human activities on sediment dynamics, floculation and
597 fluid mud layer formation at regional scale? As reported in the recent publications of Schmitt
598 et al. (2017) and Thi Ha et al. (2018), human pressure, through sediment trapping and sand
599 mining, already leads to a significant decrease of SSC in the estuaries. Our study points out
600 that SSC is a determining factor affecting, first flocculation, and secondly, the formation of
601 fluid mud layers in the Mekong estuary. There is a critical treshold of around SSC = 0.4 $g.L^{-1}$,
602 that can be seen as a tipping point for sediment processes. If the occurrence of SSC beyond
603 that point decreases, the deposition rate will strongly reduce (no linear effects), while the
604 erosion rate will probably increase because of a decrease of sediment quantity, and because of
605 the reduction of drag coefficient in the regions of fluid muds (Dyer et al., 2002a), which
606 enhances boundary shear stresses nearshore, coinciding with erosional areas in the Mekong
607 estuaries (Kineke et al., 1996). As fluid mud layers in the Mekong estuaries are a key factor to

promote flocculation and "boost" natural sedimentation, we do believe that some regular monitoring programs should be realized. In terms of coastal management, a simple measure that should be seriously considered is mangrove reforestation. Because of cohesiveness, sediment particles transported out into mangrove forests during tidal inundation flocculate and form larger flocs. Thus mangroves are not just passive colonisers of mud banks but they are active in trapping suspended sediment, with positive feedback on shore protection (Furukawa et al., 1997; Anthony and Gratiot, 2012; Gratiot and Anthony, 2016). This mechanism was recently characterized through a deep geomorphological study conducted along the muddy coast of the Guianas. In this environment, which is comparable to the Mekong shore, Brunier et al. (2019) observed and quantified some exceptional rates of muddy shoreline retreat following mangrove removal for field rice production. Apart from this mechanism, mangroves play a role as a buffer between sea and land to prevent river sediment from re-entrainment to the ocean at ebb tide (Furukawa and Wolanski, 1996).

5. Conclusions

Field surveys and laboratory analysis were performed at regional scale in the upper fluvial, lacustrine and lower estuarine environments to provide a physically-based assessment of sediment transport regimes, flocculation, and fluid mud layer dynamics along the Lower Mekong River (LMR). The independent evaluation of particle size and settling velocity provides a good assessment of particles behaviour, and allows characterizing the R_o number and corresponding regimes in a robust way. Suspended sediments in fluvial and lacustrine environments are predominantly flocculi (97 % and 100 % of total volume, respectively) and primary particles, the modes are transported as washload or with a regime of strong suspension. Some of these particles (primary particles and flocculi) probably experience phases of deposition and resuspension, mostly in the adjacent floodplain, during their routing through the Mekong basin, but we observed comparable sub distributions for fluvial, lacustrine and even estuarine environments. This finding indicates that the primary particles and flocculi populations very probably reach the estuary without any important physical transformations (i.e. with similar PSD). In the estuary, the complex mixing between fluvial and coastal waters and sediments offers optimal conditions of salinity, that leads to a higher diversity of particles, with significant proportions of microflocs and macroflocs (25 % of total volume), in the sand size range (diameter > 300 µm).

639 The original estimation of flocculation indexes with SCAF instrument allows defining clearly
640 the flocculation regime. This later is the most efficient for SSC in the range of 0.4 – 4 $g.L^{-1}$. In
641 fluvial, lacustrine and estuarine environments, flocculation regime develops for the same
642 range of SSC, beyond ~0.4 $g.L^{-1}$. Flocculation then becomes a key process, but its impacts on
643 particles populations differs with the different environments. In the Tonle Sap lake,
644 flocculation promotes the aggregation of colloids and primary particles on flocculi. In the
645 estuarine environment, flocculation leads to the formation of a new population of particles, the
646 micro-flocs. In the fluvial environment, the data were too scarce to draw a clear conclusion, as
647 freshly eroded aggregates could not be yet in equilibrium with river hydro-sedimentary
648 conditions.

649 As a consequence of these microscopic changes at scales of particles, our study confirms the
650 regular occurrence of fluid mud layers (55 - 60% of occurrence) near bottom in the Mekong
651 delta with distance of less than 120 km from the coastline, concentrated in 30 km in both high
652 - and low - flow seasons. Fluid mud layers, which are intrinsically linked with flocculation
653 processes, are early steps of landforms evolutions and participate to the geomorphology of the
654 Mekong Delta (MD). In the light of this study and considering the degree of vulnerability of
655 the delta to ongoing hydro-sedimentary changes, we may provide two recommendations:
656 Firstly, the continental sediment flux needs to be restored (or at least maintained) and human
657 driven subsidence needs to be controlled. Under those conditions, fluid mud layers should
658 remain a driver of river and coastal geomorphology, as it has been the case over the last
659 millennia. Secondly, the perception of mangrove should be reconsidered as reforestation is
660 probably the optimal manner, in both technical and environmental aspects, for ensuring
661 sediment trapping and preserving fluid mud layers and mudflat, with positive feedbacks on
662 mangrove colonization. In other words, mangroves cannot compensate regional
663 disequilibrium in sediment balance, but they can facilitate the transformation of diluted
664 suspended sediment into fluid mud layers.

665 Taking into account the degree of uncertainty of field and laboratory measurements with
666 natural fresh sediments, and the degree of variability of sediment properties in such large and
667 human-impacted systems, there is a clear interest to adopt a monitoring strategy that would
668 extend the study in time and space.

669

Acknowledgements

The authors would like to thank the Université catholique de Louvain, Belgium for Hoang-Anh Le's doctoral fellowship, the Institut de Recherche pour le Développement (IRD - France) to support the field surveys in Laos and in Vietnam with the financial support of the Lower Mekong Delta coastal zones project (http://lmdcz.siwrr.org.vn). We also would like to thanks VolTransMESKONG CNES/TOSCA project to support the monitoring in Cambodia with the technical and scientific support of staff from LOG UMR8187 and the Institute of Technology of Cambodia, especially.

References

1. Anthony, E. J., & Gratiot, N. (2012). Coastal engineering and large-scale mangrove destruction in Guyana, South America: Averting an environmental catastrophe in the making. Ecological Engineering, 47, 268-273.
2. Anthony, E.J., (2015). Wave influence in the construction, shaping and destruction of river deltas: A review. Marine Geology, 361, 53-78.
3. Antoine, G., Cazilhac, M., Monnoyer, Q., Jodeau, M., Gratiot, N., Besnier, A. L., ... & Le Brun, M. (2015, April). Lateral and vertical heterogeneity of flow and suspended sediment characteristics during a dam flushing event, in high velocity conditions. In EGU General Assembly Conference Abstracts (Vol. 17).
4. Azhikodan, G., & Yokoyama, K. (2018). Sediment transport and fluid mud layer formation in the macro-tidal Chikugo river estuary during a fortnightly tidal cycle. Estuarine, Coastal and Shelf Science, 202, 232-245.
5. Azrulhisham, E. A., & Azri, M. A. (2018, February). Application of LISST instrument for suspended sediment and erosive wear prediction in run-of-river hydropower plants. In 2018 IEEE International Conference on Industrial Technology (ICIT) (pp. 886-891). IEEE.
6. Bachmann, R. W., Hoyer, M. V., Vinzon, S. B., & Daniel Jr, E. C. (2005). The origin of the fluid mud layer in Lake Apopka, Florida. Limnology and Oceanography, 50(2), 629-635.
7. Balica, S., Dinh, Q., Popescu, I., Vo, T. Q., & Pham, D. Q. (2014). Flood impact in the Mekong delta, Vietnam. Journal of Maps, 10(2), 257-268.

8. Brunier, G., Anthony, E. J., Gratiot, N., & Gardel, A. (2019). Exceptional rates and mechanisms of muddy shoreline retreat following mangrove removal. Earth Surface Processes and Landforms.
9. Camenen, B., & van Bang, D. P. (2011). Modelling the settling of suspended sediments for concentrations close to the gelling concentration. Continental Shelf Research, 31(10), S106-S116.
10. Camenen, B., Le Coz, J., Dramais, G., Peteuil, C., Fretaud, T., Falgon, A., ... & Moore, S. A. (2014). A simple physically-based model for predicting sand transport dynamics in the Lower Mekong River. In Proc. River Flow conference, Lausanne, Switzerland, 8p.
11. Castro-Orgaz, O., Giráldez, J. V., Mateos, L., & Dey, S. (2012). Is the von Kármán constant affected by sediment suspension?. Journal of Geophysical Research: Earth Surface, 117(F4).
12. Comba, S., & Sethi, R. (2009). Stabilization of highly concentrated suspensions of iron nanoparticles using shear-thinning gels of xanthan gum. Water Research, 43(15), 3717-3726.
13. Darby, S. E., Hackney, C. R., Leyland, J., Kummu, M., Lauri, H., Parsons, D. R., ... & Aalto, R. (2016). Fluvial sediment supply to a mega-delta reduced by shifting tropical-cyclone activity. Nature, 539(7628), 276.
14. Droppo, I. G., Nackaerts, K., Walling, D. E., & Williams, N. (2005). Can flocs and water stable soil aggregates be differentiated within fluvial systems?.Catena, 60(1), 1-18.
15. Dyer, K. R., Bale, A. J., Christie, M. C., Feates, N., Jones, S., & Manning, A. J. (2002). The turbidity maximum in a mesotidal estuary, the Tamar Estuary, UK: I. Dynamics of suspended sediment. In Proceedings in Marine Science (Vol. 5, pp. 203-218). Elsevier.
16. Dyer, K. R., Bale, A. J., Christie, M. C., Feates, N., Jones, S., & Manning, A. J. (2002b). The turbidity maximum in a mesotidal estuary, the Tamar estuary, UK: II. The floc properties. In Proceedings in Marine Science (Vol. 5, pp. 219-232). Elsevier.
17. Edmonds, D. A., & Slingerland, R. L. (2010). Significant effect of sediment cohesion on delta morphology. Nature Geoscience, 3(2), 105.
18. Eidam, E. F., Nittrouer, C. A., Ogston, A. S., DeMaster, D. J., Liu, J. P., Nguyen, T. T., & Nguyen, T. N. (2017). Dynamic controls on shallow clinoform geometry: Mekong Delta, Vietnam. Continental Shelf Research, 147, 165-181.
19. Farrell, E. J., & Sherman, D. J. (2013). Estimates of the Schmidt Number for vertical flux distributions of wind-blown sand. Journal of Coastal Research, 65(sp2), 1289-1295.

20. Fennessy, M. J., Dyer, K. R., & Huntley, D. A. (1994). Size and settling velocity distributions of flocs in the Tamar Estuary during a tidal cycle. Netherland Journal of Aquatic Ecology, 28(3-4), 275-282.
21. Fettweis, M., Francken, F., Pison, V., & Van den Eynde, D. (2006). Suspended particulate matter dynamics and aggregate sizes in a high turbidity area. Marine Geology, 235(1-4), 63-74.
22. Furukawa, K., & Wolanski, E. (1996). Sedimentation in mangrove forests. Mangroves and Salt Marshes, 1(1), 3-10.
23. Furukawa, K., Wolanski, E., & Mueller, H. (1997). Currents and sediment transport in mangrove forests. Estuarine, Coastal and Shelf Science, 44(3), 301-310.
24. Gabioux, M., Vinzon, S. B., & Paiva, A. M. (2005). Tidal propagation over fluid mud layers on the Amazon shelf. Continental Shelf Research, 25(1), 113-125.
25. Gratiot, N., Gardel, A. and Anthony, E.J., 2007. Trade-wind waves and mud dynamics on the French Guiana coast, South America: input from ERA-40 wave data and field investigations. Marine Geology. 236, 15-26.
26. Gratiot, N., Coulaud, C., Legout, C., Mercier, B., Mora, H., & Wendling, V. (2015). Unit for measuring the falling speed of particles in suspension in a fluid and device comprising at least one measuring unit and one automatic sampler. Patent - Publication number WO2015055963 A, 1.
27. Gratiot, N., & Anthony, E. J. (2016). Role of flocculation and settling processes in development of the mangrove-colonized, Amazon-influenced mud-bank coast of South America. Marine Geology, 373, 1-10.
28. Gratiot, N., Bildstein, A., Anh, T. T., Thoss, H., Denis, H., Michallet, H., & Apel, H. (2017). Sediment flocculation in the Mekong River estuary, Vietnam, an important driver of geomorphological changes. Comptes Rendus Geoscience, 349(6-7), 260-268.
29. Gugliotta, M., Saito, Y., Nguyen, V. L., Ta, T. K. O., & Tamura, T. (2019). Sediment distribution and depositional processes along the fluvial to marine transition zone of the Mekong River delta, Vietnam. Sedimentology, 66(1), 146-164.
30. Gupta, A., & Liew, S. C. (2007). The Mekong from satellite imagery: A quick look at a large river. Geomorphology, 85(3-4), 259-274.
31. Hai, P. T., Masumoto, T., & Shimizu, K. (2008). Development of a two-dimensional finite element model for inundation processes in the Tonle Sap and its environs. Hydrological Processes: An International Journal, 22(9), 1329-1336.

766 32. Hung, N. N., Delgado, J. M., Güntner, A., Merz, B., Bárdossy, A., & Apel, H. (2014).
767 Sedimentation in the floodplains of the Mekong Delta, Vietnam Part II: deposition and
768 erosion. Hydrological Processes, 28(7), 3145-3160.
769 33. Kineke, G. C., Sternberg, R. W., Trowbridge, J. H., & Geyer, W. R. (1996). Fluid-mud
770 processes on the Amazon continental shelf. Continental Shelf Research, 16(5-6), 667-696.
771 34. Kondolf, G. M., Rubin, Z. K., & Minear, J. T. (2014). Dams on the Mekong: Cumulative
772 sediment starvation. Water Resources Research, 50(6), 5158-5169.
773 35. Kummu, M., & Sarkkula, J. (2008). Impact of the Mekong River flow alteration on the
774 Tonle Sap flood pulse. AMBIO: AMBIO, 37(3), 185-193.
775 36. Kummu M, Tes S, Yin S, Adamson P, Jozsa J, Koponen J, Richey J, Sarkkula J (2014)
776 Water balance analysis for the Tonle Sap Lake - floodplain system. Hydrological
777 Processes 28(4):1722-1733.
778 37. Le, H. A., Lambrechts, J., Ortled, S., Gratiot, N., Deleersnijder, E., Soares-Frazao, S.,
779 (2019). An implicit wetting - drying algorithm for the Discontinuous Galerkin method:
780 Application to the Tonle Sap, Mekong River Basin. Environmental Fluid Mechanics (in
781 submission).
782 38. Lee, B. J., Fettweis, M., Toorman, E., & Molz, F. J. (2012). Multimodality of a particle
783 size distribution of cohesive suspended particulate matters in a coastal zone. Journal of
784 Geophysical Research: Oceans, 117(C3).
785 39. Malarkey, J., Baas, J. H., Hope, J. A., Aspden, R. J., Parsons, D. R., Peakall, J., ... & Bass,
786 S. J. (2015). The pervasive role of biological cohesion in bedform development. Nature
787 communications, 6, 6257.
788 40. Manh, N.V., Dung, N.V., Hung, N.N., Merz, B., & Apel, H. (2014). Large-scale
789 quantification of suspended sediment transport and deposition in the Mekong
790 Delta. Hydrology and Earth System Sciences Discussions, 11(4).
791 41. Manh, N.V, Dung, N. V., Hung, N. N., Kummu, M., Merz, B., & Apel, H. (2015). Future
792 sediment dynamics in the Mekong Delta floodplains: Impacts of hydropower
793 development, climate change and sea level rise. Global and Planetary Change, 127, 22-33.
794 42. Manning, A. J., Friend, P. L., Prowse, N., & Amos, C. L. (2007). Estuarine mud
795 flocculation properties determined using an annular mini-flume and the LabSFLOC
796 system. Continental Shelf Research, 27(8), 1080-1095.
797 43. Manning, A. J., Baugh, J. V., Spearman, J. R., & Whitehouse, R. J. (2010). Flocculation
798 settling characteristics of mud: sand mixtures. Ocean dynamics, 60(2), 237-253.

44. Manning, A.J., Baugh, J.V., Soulsby, R.L., Spearman, J.R., Whitehouse, R.J.S., 2011a. Cohesive sediment flocculation and the application to settling flux modelling (Chapter 5). In: Ginsberg, Silvia Susana (Ed.), Sediment Transport. InTech, Vienna, ISBN: 978-953-307-189-3, pp. 91–116.
45. Manning, A. J., Baugh, J. V., Spearman, J. R., Pidduck, E. L., & Whitehouse, R. J. (2011b). The settling dynamics of flocculating mud-sand mixtures: Part 1—Empirical algorithm development. Ocean Dynamics, 61(2-3), 311-350.
46. Marchesiello, P., Nguyen, N.M., Gratiot, N., Loisel, H., Anthony, E.J. and Nguyen, T., 2019. Erosion of the coastal Mekong delta: Assessing natural against man induced processes. Continental Shelf Research, 181, 72-89.
47. McAnally, W. H., Friedrichs, C., Hamilton, D., Hayter, E., Shrestha, P., Rodriguez, H., ... & ASCE Task Committee on Management of Fluid Mud. (2007). Management of fluid mud in estuaries, bays, and lakes. I: Present state of understanding on character and behavior. Journal of Hydraulic Engineering, 133(1), 9-22.
48. McLachlan, R. L., Ogston, A. S., & Allison, M. A. (2017). Implications of tidally - varying bed stress and intermittent estuarine stratification on fine-sediment dynamics through the Mekong's tidal river to estuarine reach. Continental Shelf Research, 147, 27-37.
49. Mehta, A. J. (1991). Understanding fluid mud in a dynamic environment. Geo-Marine Letters, 11(3-4), 113-118.
50. Mekong River Commission portal, available at http://www.mrcmekong.org/.
51. Mikkelsen, O. A., Hill, P. S., & Milligan, T. G. (2006). Single-grain, microfloc and macrofloc volume variations observed with a LISST-100 and a digital floc camera. Journal of Sea Research, 55(2), 87-102.
52. Milliman, J. D., & Meade, R. H. (1983). World-wide delivery of river sediment to the oceans. The Journal of Geology, 91(1), 1-21.
53. Nguyen, T. T., Némery, J., Gratiot, N., Garnier, J., Strady, E., Tran, V. Q., ... & Aimé, J. (2019). Phosphorus adsorption/desorption processes in the tropical Saigon River estuary (Southern Vietnam) impacted by a megacity. Estuarine, Coastal and Shelf Science, 106321.
54. Nittrouer, C. A., DeMaster, D. J., Eidam, E. F., Nguyen, T. T., Liu, J. P., Ogston, A. S., & Phung, P. V. (2017). The Mekong continental shelf: The primary sink for deltaic sediment particles and their passengers. Oceanography, 30(3), 60-70.

831 55. Nowacki, D. J., Ogston, A. S., Nittrouer, C. A., Fricke, A. T., & Van, P. D. T. (2015).
832 Sediment dynamics in the lower Mekong River: Transition from tidal river to
833 estuary. Journal of Geophysical Research: Oceans, 120(9), 6363-6383.
834 56. Parsons, D. R., Schindler, R. J., Hope, J. A., Malarkey, J., Baas, J. H., Peakall, J., ... &
835 Aspden, R. J. (2016). The role of biophysical cohesion on subaqueous bed form
836 size. Geophysical research letters, 43(4), 1566-1573.
837 57. Peteuil, C., Frétaud, T., Wirz, C., Camenen, B., Guertault, L., Le Coz, J., & Dramais, G.
838 (2014). Importance of field observation for managing sediment fluxes in hydropower
839 projects design and operation. In Proceedings of the 19th IAHR-APD Congress, Hanoi,
840 Vietnam.
841 58. Ribolzi, O., Evrard, O., Huon, S., Rouw, A. De, Silvera, N., Latsachack, O., Soulileuth, B.,
842 Lefèvre, I., Pierret, A., 2017. From shifting cultivation to teak plantation : effect on
843 overland flow and sediment yield in a montane tropical catchment. Sci. Rep. 1–12.
844 59. Rijn, L. C. V. (1984). Sediment transport, part II: suspended load transport. Journal of
845 Hydraulic Engineering, 110(11), 1613-1641.
846 60. Rouse, H. (1937). Modern conceptions of the mechanics of fluid turbulence. Trans
847 ASCE, 102, 463-505.
848 61. Santini, W., Camenen, B., Coz, J. L., Vauchel, P., Guyot, J. L., Lavado, W., ... & Espinoza
849 Villar, R. (2019). An index concentration method for suspended load monitoring in large
850 rivers of the Amazonian foreland. Earth Surface Dynamics, 7(2), 515-536.
851 62. Schindler, R. J., Parsons, D. R., Ye, L., Hope, J. A., Baas, J. H., Peakall, J., ... & Paterson,
852 D. M. (2015). Sticky stuff: Redefining bedform prediction in modern and ancient
853 environments. Geology, 43(5), 399-402.
854 63. Schmitt, R. J. P., Rubin, Z., & Kondolf, G. M. (2017). Losing ground-scenarios of land
855 loss as consequence of shifting sediment budgets in the Mekong
856 Delta. Geomorphology, 294, 58-69.
857 64. Schelske, C. L. (2006). Comment on the origin of the “fluid mud layer” in Lake Apopka,
858 Florida. Limnology and Oceanography, 51(5), 2472-2480.
859 65. Seah, K. C., Qasim, G. H., Hong, Y. S., Kim, E., Kim, K. T., & Han, S. (2017).
860 Assessment of colloidal copper speciation in the Mekong River Delta using diffusive
861 gradients in thin film techniques. Estuarine, Coastal and Shelf Science, 188, 109-115.
862 66. Sequioa. LISST-Portable|XR User's Manual Version 1.2 (2016).
863 67. Siev S, Paringit EC, Yoshimura C, Hul S (2016) Seasonal Changes in the Inundation Area
864 and Water Volume of the Tonle Sap River and Its Floodplain. Hydrology 3(4):33-45.

865 68. Sim, S. Y., Chan, D. C. H., Huang, T. F., Chai, W., Isaacson, T., Flood Jr, J. C., ... &
866 Orzen, M. (2007). U.S. Patent No. 7,272,613. Washington, DC: U.S. Patent and
867 Trademark Office.
868 69. Sime, L. C., Ferguson, R. I., & Church, M. (2007). Estimating shear stress from moving
869 boat acoustic Doppler velocity measurements in a large gravel bed river. Water Resources
870 Research, 43(3).
871 70. Smardon, R. (2009). Restoration of the Tram Chim National Wildlife Preserve, Vietnam.
872 Sustaining the World's Wetlands, 153–178.
873 71. Sottolichio, A., Hurther, D., Gratiot, N., Bretel, P., 2011. Acoustic turbulence
874 measurements of near-bed suspended sediment dynamics in highly turbid waters of a
875 macrotidal estuary. Continental Shelf Research, 31, S36-S49.
876 72. Spearman, J., & Manning, A. J. (2008). On the significance of mud transport algorithms
877 for the modelling of intertidal flats. In Proceedings in Marine Science (Vol. 9, pp. 411-
878 430). Elsevier.
879 73. Stokes, G. G. (1857). On the effect of wind on the intensity of sound. Brit. Assoc.
880 Report, 22.
881 74. Ta, T. K. O., Nguyen, V. L., Tateishi, M., Kobayashi, I., Tanabe, S., & Saito, Y. (2002).
882 Holocene delta evolution and sediment discharge of the Mekong River, southern
883 Vietnam. Quaternary Science Reviews, 21(16-17), 1807-1819.
884 75. Thi Ha, D., Ouillon, S., & Van Vinh, G. (2018). Water and suspended sediment budgets in
885 the lower Mekong from high-frequency measurements (2009–2016). Water, 10(7), 846.
886 76. Toorman, E.A., Anthony, E., Augustinus, P.G.E.F., Gardel, A., Gratiot, N., Homenauth,
887 O., Huybrechts, N., Monbaliu, J., Moseley, K., Naipal, S. 2018. Interaction of mangroves,
888 coastal hydrodynamics and morphodynamics along the coastal fringes of the Guianas.
889 Coastal research library series, Springer book, pp 429-473.
890 77. Tran, D. D., Van Halsema, G., Hellegers, P. J., Hoang, L. P., Tran, T. Q., Kummu, M., &
891 Ludwig, F. (2018). Assessing impacts of dike construction on the flood dynamics of the
892 Mekong Delta. Hydrology and Earth System Sciences, 22(3).
893 78. Tri, V. K. (2012). Hydrology and hydraulic infrastructure systems in the Mekong Delta,
894 Vietnam. In The Mekong Delta System (pp. 49-81). Springer, Dordrecht.
895 79. Udo, K., & Mano, A. (2011). Application of Rouse's Sediment Concentration Profile to
896 Aeolian Transport: Is the suspension system for sand transport in air the same as that in
897 water?. Journal of Coastal Research, 2079-2083.

80. Uncles, R. J., Stephens, J. A., & Law, D. J. (2006). Turbidity maximum in the macrotidal, highly turbid Humber Estuary, UK: Flocs, fluid mud, stationary suspensions and tidal bores. Estuarine, Coastal and Shelf Science, 67(1-2), 30-52.

81. Van, L. A., & Van Bang, D. P. (2013). Hindered settling of sand–mud flocs mixtures: From model formulation to numerical validation. Advances in Water Resources, 53, 1-11.

82. Van Leussen, 1994. Estuarine macroflocs and their role in fine-grained sediment transport. Ph.D. thesis, University of Utrecht, The Netherlands.

83. Vanoni, V. A. (1946). Transportation of suspended sediment by water. Trans. of ASCE, 111, 67-102.

84. W.C. Rouse. U.S. Patent and Trademark Office (1938).

85. Wendling, V., Gratiot, N., Legout, C., Droppo, I. G., Coulaud, C., & Mercier, B. (2015). Using an optical settling column to assess suspension characteristics within the free, flocculation, and hindered settling regimes. Journal of Soils and Sediments, 15(9), 1991-2003.

86. Windt, C., Ebrahimian, A., & Traver, R. Flow Characterization of Stormwater Runoff in Philadelphia. In World Environmental and Water Resources Congress 2017 (pp. 365-371).

87. Winterwerp, J. C. (2002). On the flocculation and settling velocity of estuarine mud. Continental Shelf Research, 22(9), 1339-1360.

88. Winterwerp, J. C. (2011). Fine sediment transport by tidal asymmetry in the high-concentrated Ems River: indications for a regime shift in response to channel deepening. Ocean Dynamics, 61(2-3), 203-215.

89. Wolanski, E., Huan, N. N., Nhan, N. H., & Thuy, N. N. (1996). Fine-sediment dynamics in the Mekong River estuary, Vietnam. Estuarine, Coastal and Shelf Science, 43(5), 565-582.

90. Wolanski, E., Nhan, N. H., & Spagnol, S. (1998). Sediment dynamics during low flow conditions in the Mekong River estuary, Vietnam. Journal of Coastal Research, 472-482.

91. Xing, F., Meselhe, E. A., Allison, M. A., & Weathers III, H. D. (2017). Analysis and numerical modeling of the flow and sand dynamics in the lower Song Hau channel, Mekong Delta. Continental Shelf Research, 147, 62-77.

Appendix

Fig. a, b, c display the detailed PSD for some representative samples collected in fluvial, lacustrine and estuarine environments, respectively. For clarity purposes, only a limited (nine) number of samples are represented in the first panel row. The second row exhibits representative PSDs without sonication and the last row is for representative PSDs with sonication. After two minutes of sonication, all three environments show higher percentages of smallest constituents, namely primary particles. The mean size of samples taken in the fluvial and lacustrine parts is smaller than ones taken in the estuary, especially after sonication, a considerable constituent of primary particles is found in the upper parts. In addition, the particle size in Tonle Sap was smallest, with mean diameter of approximately 7 µm and primary particles are predominance. In contrast, the graphs illustrate the large variation of particle sizes in the delta, predominantly in range of 10 - 386 µm before sonication and 2.21 - 331 µm after sonication. It is clear that sand appears in the Mekong estuary with percentage of 11 %; a median diameter of > 300 µm.

(a) Fluvial — Mekong river, Laos, 06/2017

(b) Lacustrine — Tonle Sap, Cambodia, 09/2018

(c) Estuarine — Mekong estuary, Vietnam, 03/2016

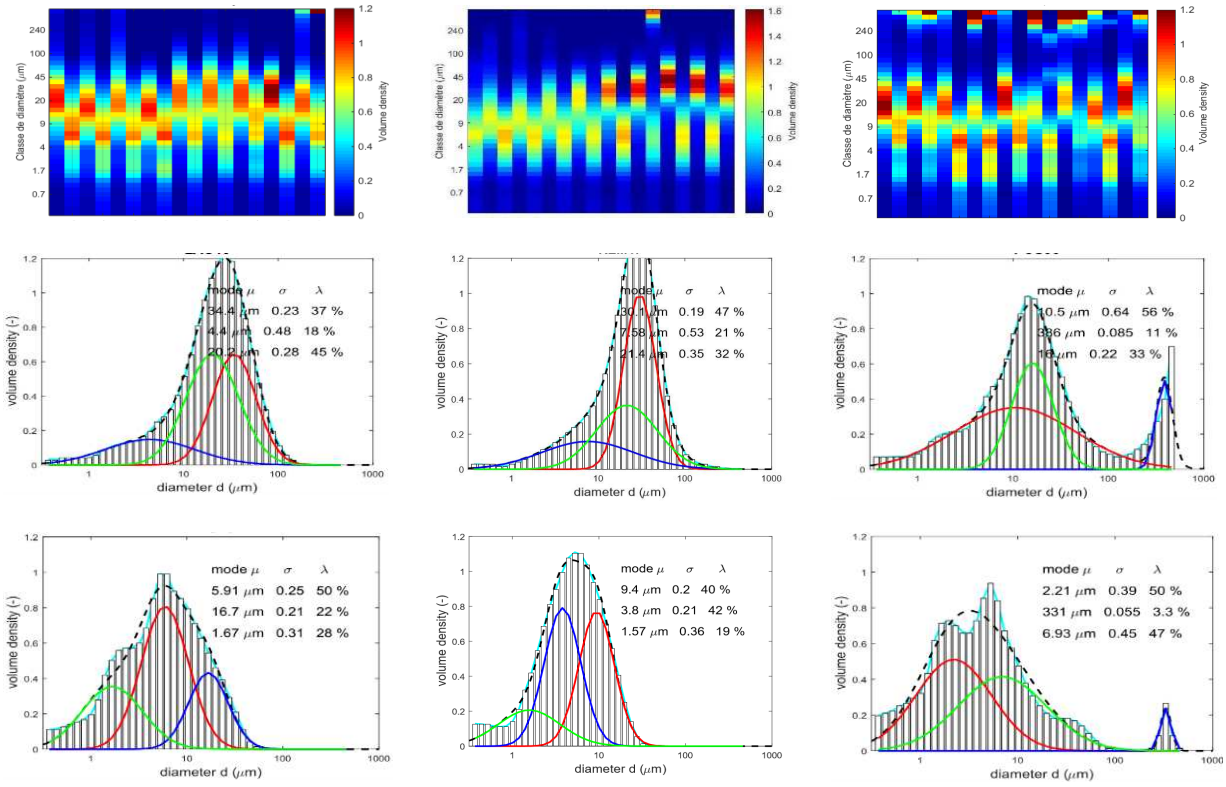

Fig. PSD of three representative samples in fluvial, lacustrine and estuary environments